ORIGINAL PAPER

Investigation of alumina nanoparticles role on the critical flux and performance of polyvinyl chloride membrane in a submerged membrane system for the removal of humic acid

Habib Etemadi[1] · Hamidreza Qazvini[1]

Abstract

In this work, the polyvinyl chloride/alumina (PVC/Al_2O_3) ultrafiltration (UF) nanocomposite membranes were prepared with different amounts of Al_2O_3 within a range of 0–2 wt.%. Neat PVC and optimum nanocomposite membranes were evaluated in a submerged membrane system for the removal of humic acid (HA). The Fourier transform infrared (FTIR) spectroscopy confirmed the presence of hydroxyl group (OH) on the surface of the PVC nanocomposite membrane. Results revealed that the nanocomposite membrane with 1.5 wt.% of Al_2O_3 nanoparticles has the highest value in porosity and hydrophilicity when compared to other samples. The results obtained from the field emission scanning electron microscopy (FE-SEM) images showed that as Al_2O_3 was added to the membrane structure, more pores and larger pores were formed on the membrane surface. A higher critical flux was obtained by the PVC/Al_2O_3 (1.5 wt.%) nanocomposite membrane due to change in the surface characteristics. Antifouling analysis under subcritical conditions for neat PVC membrane showed that the main portion of the total fouling ratio was irreversible fouling ratio (IFR), while the nanocomposite membrane with 1.5 wt.% of Al_2O_3 nanoparticles significantly decreased IFR. Finally, the nanocomposite membrane had a higher HA rejection than the neat PVC membrane.

Keywords Polyvinyl chloride membrane · Alumina nanoparticles · Submerged membrane system · Critical flux · Antifouling

✉ Habib Etemadi
    h_etemadi@ubonab.ac.ir

[1] Department of Polymer Science and Engineering, University of Bonab, Bonab, Iran

Introduction

On account of strict regulations on the distributed water quality as well as a globally increasing demand for as a result of demographic and industrial growth, the membrane technology is widely used for water treatment and reuse, due to its low energy consumption, easy scale-up, less or no use of chemicals, low maintenance cost, significant decrease in conductivity and absence of any harmful byproduct formation [1–4]. In this case, ultrafiltration (UF, the low-pressure membrane process) has received considerable attention in recent years [5]. However, membrane fouling is one of the major obstacles in the way of successful application of membrane systems for water treatment [6, 7].

According to the literature, natural organic matters (NOM) constitute a major membrane-fouling agent in the UF process for the treatment of surface waters [8, 9]. Humic acid (HA) is a major fraction of dissolved NOM and a degradation product of lignin, carbohydrate and protein with high molecular weight, which is often present in surface waters [10].

Various polymers such as polyethersulfone (PES) [11], polysulfone (PSf) [12], cellulose acetate (CA) [13], polyvinylidene fluoride (PVDF) [14] and polyvinyl chloride (PVC) [6] are used in membrane preparation for the removal of HA in contaminated surface waters. Among them, PVC is widely used for the fabrication of UF membranes because of its excellent chemical stability, high thermal and mechanical properties as well as low cost in comparison with others [15, 16]. However, the hydrophobic nature of PVC results in membranes with high fouling propensity, which is of great concern over its potentially practical application [15, 17]. Therefore, membrane modifications seem to be essential to improve the antifouling properties of PVC membranes.

Several studies have reported the use of nanoparticles in the preparation of PVC nanocomposite membranes with improved antifouling properties. In this regard, various nanoparticles such as titanium oxide (TiO_2) [18], silver [15], zinc oxide (ZnO) [16], Fe_2O_3 [19] and graphene oxide (GO) [20] were used in the preparation of PVC nanocomposite membrane.

Alumina (Al_2O_3) nanoparticles are one of the most attractive engineering ceramics with a variety of applications in various industries. It is used as a filler in membrane preparation because of hydrophilicity and concomitant interesting chemical, mechanical and thermal properties [21]. Compared to many other nanoparticles such as carbon nanotube (CNT), Al_2O_3 nanoparticles have attracted the attention of researchers for obtaining high-performance nanocomposite membranes with antifouling properties, due to interesting characteristics as well as low costs.

Homayoonfa et al. [22] investigated the effect of Al_2O_3 on the performance and anti-biofouling properties of PSf membranes in membrane bioreactor (MBR). They concluded that Al_2O_3 nanoparticles can increase water flux by enhancing the membrane hydrophilicity and reduce biofilm formation on the membrane surface. The effect of Al_2O_3 nanoparticles on the performance of polyamide (PA) membrane was examined by Saleh et al. [23]. They found from water flux and

salt rejection results that the performance of nanocomposite membrane was better than that of the pristine membrane. In other research, Yan et al. [24] observed that incorporation of Al_2O_3 nanoparticles in PVDF membrane for oily wastewater treatment led to a significant improvement in the membrane antifouling performance. Recently, Ghazanfari et al. [25] used Al_2O_3 nanoparticles in order to improve the antifouling properties of the PVC membrane in the MBR system. They reported incorporation of Al_2O_3 reduced membrane fouling, but they did not present any report about the surface porosity of the PVC membrane. However, the operational conditions (such as critical flux determination) investigation on the role of Al_2O_3 nanoparticles in the antifouling performance of PVC membranes in a submerged membrane system for HA filtration is very limited in the open literature. Generally, membrane fouling is affected by the chemical properties of HA and the membrane as well as the operating conditions. It was found that the desired surface interactions and the enhancement of convective transport of HA to membrane surface both result in an increase in the membrane fouling [26].

Our study aimed to prepare PVC/Al_2O_3 nanocomposite membrane in a submerged membrane system for HA removal. According to many reports from the literature, PVC nanocomposite membrane, which has been prepared by various nanoparticles such as graphene oxide (GO) [20], ZnO [16], TiO_2 [27] and GO–TiO_2 [6], showed a surface with low porosity or very small pore size on the nanocomposite membrane surface. In this study, we show that Al_2O_3 nanoparticles are a good candidate for improving the hydrophilicity and the surface porosity of the PVC membrane with a larger pore size. Meanwhile, up to now, many works about HA removal from contaminated water and determining the critical flux have been focused on dead-end or cross-flow filtration systems. Operation conditions have a critical role on the membrane fouling and subsequently operational costs. In this case, critical flux was determined in order to perform membrane operation under subcritical conditions. So, in this work, critical flux and membrane fouling for both neat PVC and PVC/Al_2O_3 nanocomposite membranes were examined under subcritical flux conditions in a submerged membrane system for the first time.

Experimental

Materials

Polyvinyl chloride (MW = 90,000), which was used as a polymer material for preparing PVC membrane, was supplied by Arvand Petrochemical Company, Iran. Al_2O_3 nanoparticles (gamma phase) were procured from US Research Nanomaterials, Inc., with an average diameter of 20 nm. Polyethylene glycol (PEG) with molecular weight of 200 Da and 1-methyl 2-pirrolidone (NMP) were supplied from Merck and used as pore former and polymer solvent for the membrane preparation, respectively. Deionized (DI) water was used as non-solvent. HA as common water contaminant was purchased from Sigma-Aldrich in order to investigate the membrane-fouling behavior.

Preparation of membranes

Neat PVC and nanocomposite membranes were prepared by the non-solvent-induced phase separation (NIPS) method. Firstly, Al_2O_3 nanoparticles were dried at 85 °C for 6 h under vacuum conditions to remove any possible physically absorbed moisture. Different amounts of nanoparticles were added to NMP and stirred by a magnetic stirrer for 2 h at room temperature. The mixture was then sonicated by ultrasonic bath at 50 kHz for 2 h to obtain a homogeneous dispersion of the nanoparticles. Then, the PVC polymer and PEG were added to the homogenous suspension under constant stirring for at least 24 h until a homogeneous solution was obtained. After complete degassing for 24 h, the casting solution was cast on glass plates with a steel knife with a gap of 150 μm and immersed in a water coagulation bath. The cast film is instantaneously immersed in a DI water bath for 24 h to complete the phase inversion process. The details of the solution dope compositions are listed in Table 1.

Membrane characterization

SEM analysis

The surface and cross-sectional morphologies of the prepared neat PVC and PVC/Al_2O_3 membranes were studied by field emission scanning electron microscopy (FE-SEM; MIRA3 FEG-SEM, Tescan) operating at 15 kV. For cross-sectional images, the membranes were fractured in liquid nitrogen. The FE-SEM device was equipped with an energy-dispersive X-ray (EDX) analysis detector to inspect the existence of Al_2O_3 nanoparticles as well as dispersion nanoparticles within the membranes.

TEM analysis

In order to show dispersion state of nanoparticles, transmission electron microscopy (TEM) analysis was performed with a Philips CM120 transmission electron microscope operating at 120 keV. The sample membranes were embedded with epoxy, and cross sections of approximately 50 nm were obtained by sectioning with a Leica Ultracut UCT ultramicrotome.

Table 1 Summary of the membrane composition	Membrane	Polymer and Al_2O_3 (15 wt.%)			Solvent (85 wt.%)
		PVC	PEG	Al_2O_3	NMP
	PVC	92	8	0	85
	PVC/Al-0.5	91.5	8	0.5	85
	PVC/Al-1	91	8	1	85
	PVC/Al-1.5	90.5	8	1.5	85
	PVC/Al-2	90	8	2	85

FTIR analysis

The chemical structure of nanoparticles and membranes was studied by Fourier transform infrared spectroscopy (FTIR) with a FTIR Shimadzu (IRAffinity-1S) spectrometer within a range of 400–4000 cm^{-1}. The sample pellet of nanoparticles for the FTIR test was prepared by mixing the particles with KBr. The membrane samples were placed active-face down on ATR crystal and held in place by a clamp.

Contact angle measurement

The hydrophilicity of the membranes was measured by static surface contact angle goniometer (PGX, Thwing-Albert Instrument Co., USA) in a sessile drop model at room temperature. The obtained results were the average of at least five tests at different locations on the membrane surface.

Membrane porosity

The porosity (ε, %) of membranes can be determined by the gravimetric method as shown in Eq. (1) [28]:

$$\varepsilon(\%) = \frac{(W_w - W_d)/D_w}{(W_w - W_d)/D_w + W_d/D_p} \times 100 \tag{1}$$

where W_w and W_d are weights of wet (for 24 h in water) and dry (at 65 °C for 6 h) membranes (g), respectively. D_w (0.998 g cm^{-3}) and D_p (1.3 g cm^{-3}) are the density of water and polymer, respectively.

Mechanical tensile strength

The mechanical strength of neat PVC and nanocomposite membranes was evaluated using a tensile testing machine (Santam STM-5, Iran) at an extension rate of 10 mm/min. The results were the average of at least three tests.

Bench-scale filtration experiment

The bench-scale testing unit used in this study was a submerged membrane system with a 3-L effective volume that allowed two membranes to be tested simultaneously. A schematic illustration of the setup is shown in Fig. 1. Flat sheet membrane modules were made with polyamide with a volume capacity of 50 mL and an effective membrane surface area of 14.7 cm^2. Air sparing through a diffuser, at 4 L min^{-1}, was operated from the bottom of the membrane module in order to cause a homogeneous solution as well as turbulence along the membrane surface which helps remove foulants and particles that deposit on the outside of
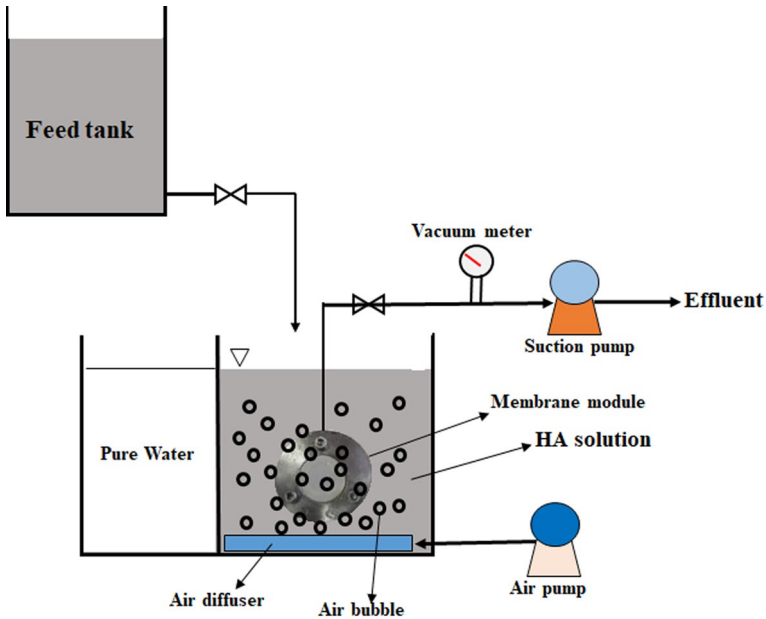
Fig. 1 Schematic representation of the submerged membrane system in this study

the membrane surface. The feed water contained 1 g/L of HA. The solution pH was adjusted at 6 by adding a small amount of either 0.1 M HCl or 0.1 M NaOH.

Critical flux determination

The critical flux (J_c) was determined according to the transmembrane pressure (TMP) step method [29, 30]. Before the experiments, membrane compaction was carried out. In this method, TMP increased with time, while the membrane flux decreased over the course of time, leading to nonlinearity in the $J=f$ (TMP) relationship, which means that hydraulic resistance increased significantly due to fouling. The critical TMP is the pressure at which the critical flux is measured.

Antifouling performance of membranes

After pure water flux (J_{w1}) tests, the flux of HA solution (J_{HA}, Lm² h⁻¹) was measured at subcritical conditions for 300 min. After HA filtration, the membrane was cleaned with distilled water and then was submerged in a pure water tank to measure the pure water flux (PWF) after fouling (J_{w2}). The flux recovery ratio (FRR) was calculated using Eq. (2) [30]:

$$\text{FRR} = \frac{J_{W2}}{J_{W1}} \times 100. \tag{2}$$

The total fouling ratio (TFR), reversible fouling ratio (RFR) and irreversible fouling ratio (IFR) were calculated using Eqs. (3)–(5) [30]:

$$RFR = \frac{J_{W2} - J_{HA}}{J_{W1}} \times 100 \tag{3}$$

$$IFR = \frac{J_{W1} - J_{W2}}{J_{W1}} \times 100 \tag{4}$$

$$TFR = FRF + IFR = \frac{J_{W1} - J_{HA}}{J_{W1}} \times 100. \tag{5}$$

In order to evaluate the effective solute separation efficiency, the HA rejection (R (%)) of membranes can be calculated using Eq. (6):

$$R(\%) = \left(1 - \frac{C_p}{C_f}\right) \times 100 \tag{6}$$

where C_p and C_f are the solute concentration (g/L) in the permeate and feed, respectively.

Results and discussion

FTIR analysis

Figure 2 shows the FTIR spectra of Al_2O_3 nanoparticles, neat PVC and PVC/Al-1.5 membranes. For Al_2O_3 nanoparticles, the peak around 3450 cm^{-1}, which results from the presence of OH group, is available in the FTIR spectrum of nanoparticles. There is also another one in 1600 cm^{-1} in Al_2O_3 nanoparticles spectrum, related to

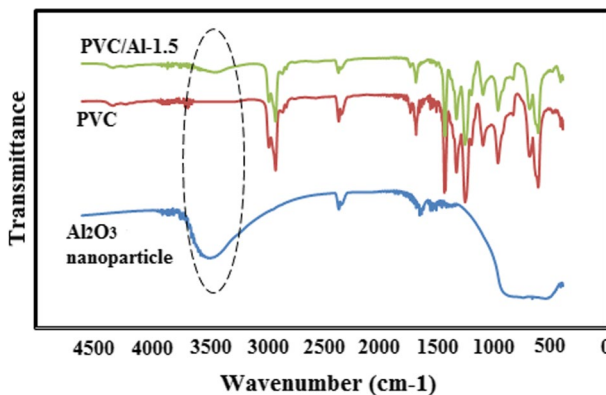**Fig. 2** FTIR spectra of Al_2O_3 nanoparticles, neat PVC and PVC/Al-1.5 membranes

the Al–O functional group [22]. A comparison between the spectrum of neat PVC and PVC/Al-1.5 nanocomposite membranes shows a peak around 3450 cm^{-1}, which confirms the presence of Al_2O_3 nanoparticles on the nanocomposite membrane surface.

Hydrophilicity, porosity and mechanical strength

In order to evaluate the effect of Al_2O_3 nanoparticles on the membrane hydrophilicity, the contact angle between of water droplet and the membrane surface was measured by a contact angle instrument, and the results are shown in Table 2. As can be seen from Table 2, the water contact angle of the neat PVC membrane was 68.5°. By increasing Al_2O_3 nanoparticles to the PVC membrane up to 1.5 wt.%, the water contact angle decreased (improvement in membrane hydrophilicity) and then increased probably due to the agglomeration of nanoparticles at 2 wt.%. Due to the presence of the hydrophilic OH group on the PVC nanocomposite membrane surface (Fig. 2), an improvement can be observed in the hydrophilicity of PVC nanocomposite. In other words, Al_2O_3 nanoparticles have a hydrophilic nature because of the presence of the OH group on their surface, and therefore, by adding Al_2O_3 nanoparticles to the PVC membrane, the membrane hydrophilicity increases. Among the PVC nanocomposite membranes, PVC/Al-1.5 shows the lowest value in the contact angle, which may be due to the good dispersion of nanoparticles in the PVC membrane.

In this work, the minimum water contact angle was 47.1°, while in other works, this value was 55.4°, 52.2°, 65° and 58° for PVC/TiO_2 [27], PVC/ZnO [16], PVC/GO [20] and PVC/TiO_2-GO [6] nanocomposite membranes, respectively. These results implied that Al_2O_3 nanoparticles significantly improved the hydrophilicity of the PVC membrane.

As given in Table 1, the nanocomposite membrane containing 1.5 wt.% nanoparticles loading has the highest values of porosity. During the phase inversion process, shrinkage of the polymer phase brings the interfacial stress between the relative hydrophobic PVC and hydrophilic Al_2O_3, which can only be released by pore formation [31]. That leads to an increase in porosity. Moreover, during the phase inversion process, the solvent and the non-solvent exchange rate increases due to the hydrophilic nature of the Al_2O_3 additive. This leads to the formation of membrane with high porosity [32]. However, when Al_2O_3 loading further increased, the membrane porosity decreased. The possible reason for the decrease in porosity at

Table 2 Water contact angle, porosity and tensile strength of neat PVC and nanocomposite membranes	Membrane	Water contact angle (°)	Porosity (%)	Tensile strength (MPa)
	PVC	68.5	66.2	9.1
	PVC/Al-0.5	53.5	69.2	8.5
	PVC/Al-1	50.6	70.9	7.4
	PVC/Al-1.5	47.1	73.6	6.7
	PVC/Al-2	51	69	6.3

the loading of 2 wt.% of nanoparticles is the agglomeration of nanoparticles on the membrane surface [13].

The effect of the Al_2O_3 content on the mechanical strengths of PVC membranes was examined, and the results are shown in Table 2. By comparing the mechanical strength of neat PVC and PVC/Al_2O_3 nanocomposite membranes, it becomes clear that all nanocomposite membranes show lower values than neat PVC membranes. It is generally accepted that incorporation of nanoparticles in UF membranes will cause a decline in the mechanical strength of membranes [33, 34]. The reason may be explained as follows: By adding nanoparticles, membrane porosity increases as well (Table 2), and therefore, the tensile strength of nanocomposite membranes decreases.

Membrane morphologies

FE-SEM was carried out to compare the morphologies of neat PVC with PVC/Al-1.5 nanocomposite membranes. The PVC/Al-1.5 nanocomposite membrane was selected as an optimum nanocomposite membrane among other samples according to hydrophilicity and porosity. The FE-SEM images were used to visualize changes in the top surface morphology after Al_2O_3 addition, and the images are shown in Fig. 3. As it can be seen, as Al_2O_3 was added to the membrane structure, more pores and larger pores were formed on the membrane surface. The surface pore sizes of PVC/Al-1.5 membrane was estimated within the range of 20–50 nm. This type of surface morphology may be due to the instantaneous demixing of membrane casting solution and rapid precipitation of the polymer matrix due to improvement in hydrophilicity.

The FE-SEM images of the cross section of neat PVC and PVC/Al-1.5 membranes are represented in Fig. 4. It can be seen that both membranes consist of three layers: top layer with a dense skin, middle layer with a finger-like structure and bottom layer with a large macrovoids structure. The thickness of the dense skin layer seems to decrease as Al_2O_3 nanoparticles were added to the solution. Also, PVC/Al-1.5 nanocomposite membranes show bigger macrovoids than neat PVC membranes. Instantaneous liquid–liquid demixing is thought to provide suitable conditions for the macrovoids formation [35]. In other words, the hydrophilic nature of Al_2O_3 nanoparticles is responsible for the rapid exchange of solvents and non-solvents during the phase separation process, which leads to the formation of bigger macrovoids in the sublayer [32]. A similar behavior has been reported elsewhere [36, 37].

In order to confirm the presence of dispersion of Al_2O_3 nanoparticles at the surface and cross section of the PVC/Al-1.5 nanocomposite membrane, the energy-dispersive spectrometry (EDS) analysis was carried out, and the results are shown in Fig. 5. From the EDS analysis of the top surface and cross section of nanocomposite membrane, the aluminum (Al) intensity (y-axis values of EDS analysis) indicates that Al_2O_3 located at the surface and cross section of nanocomposite membrane. EDX-mapping results in Fig. 5 show the dispersion quality of the Al_2O_3 nanoparticles (red dots) throughout the PVC nanocomposite membrane at the surface and cross section. As shown in Fig. 5, a
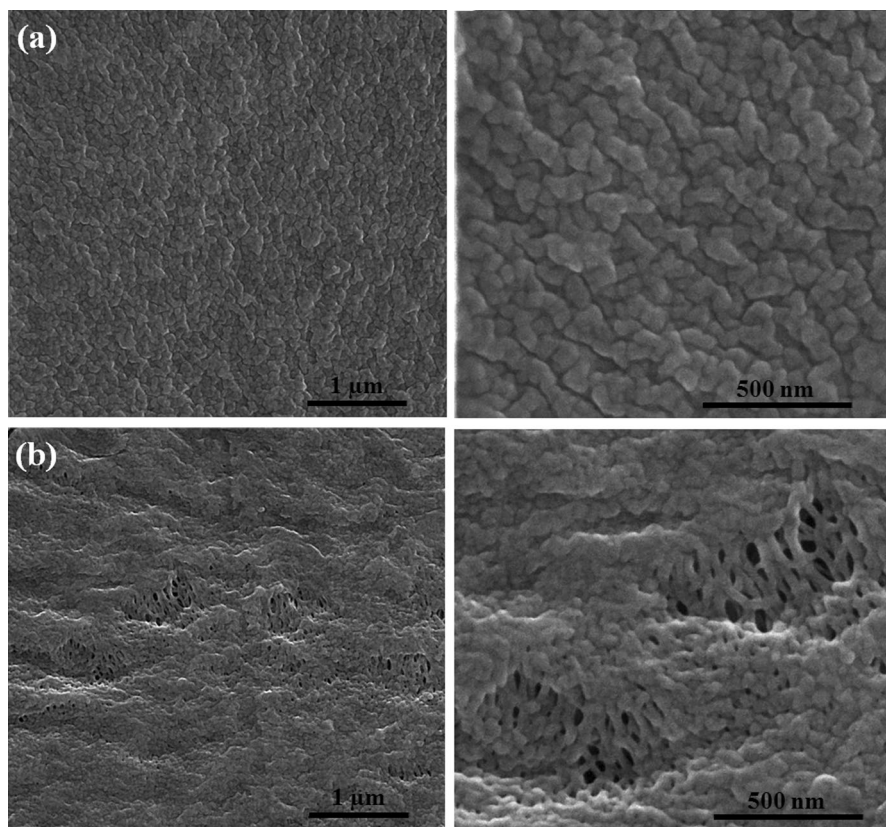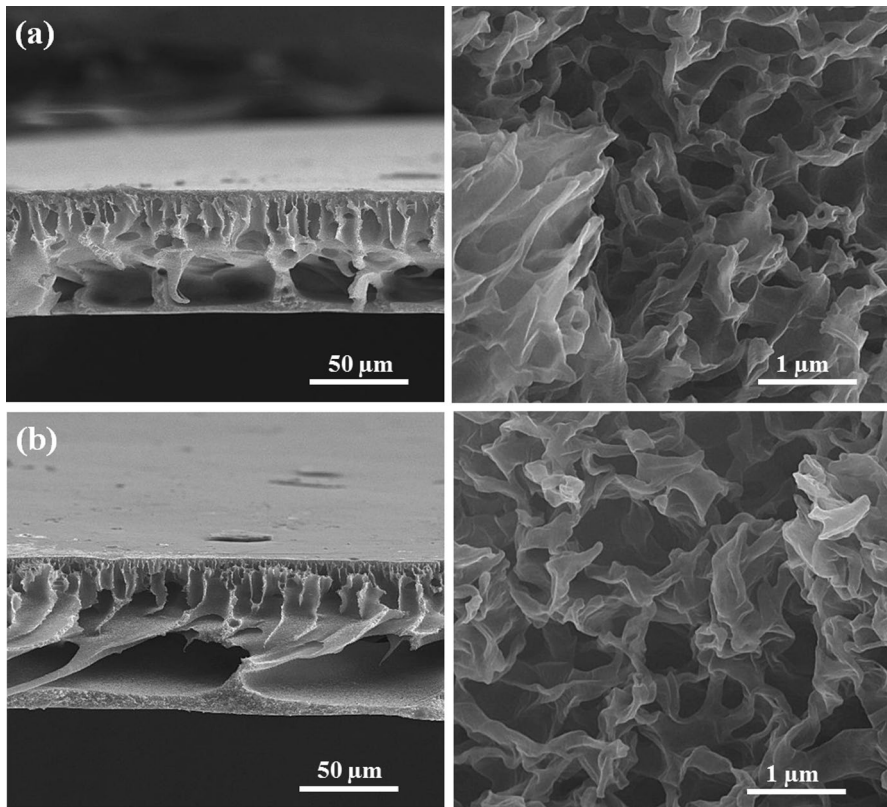
Fig. 3 FE-SEM images of membrane surface with two magnifications: **a** neat PVC, **b** PVC/Al-1.5 membranes

uniform dispersion of Al_2O_3 nanoparticles is observed at the surface and cross section of the PVC/Al-1.5 nanocomposite membrane.

However, the information about the dispersion of nanoparticles at high and low concentration of Al_2O_3 cannot be obtained from the FE-SEM images. Therefore, TEM was used to investigate the dispersion of Al_2O_3 nanoparticles in PVC membranes, and the result is shown in Fig. 6. In lower amounts of Al_2O_3 nanoparticles, i.e., 1.5 wt.%, the formation of large aggregations was prevented and therefore a relatively uniform distribution of the nanoparticles was achieved as shown in Fig. 6a. Meanwhile, by increasing the amount of nanoparticles, i.e., 2 wt.%, more agglomerations were formed (Fig. 6b).

Critical flux of neat PVC and nanocomposite membranes

The critical flux of both membranes including neat PVC and nanocomposite membranes was evaluated following the TMP step method. In this case, Fig. 7. shows the variations of permeation fluxes versus operation time for all membranes

Fig. 4 FE-SEM cross-sectional images of membrane with two magnifications: **a** neat PVC, **b** PVC/Al-1.5 membranes

using the TMP step method. As shown in Fig. 7, it is clear that the first unstable permeation fluxes for neat and all of nanocomposite membranes were obtained at 0.25 bar. According to the literature, any decrease in the permeation flux can be explained by the faster and severe fouling of membranes [38, 39]. In other words, a decrease in the permeation flux at constant TMP can be attributed to an increase in interaction between the membrane and fouling agents, which results in the formation of cake layer on the membrane surface. According to Fig. 6a, the average permeate flux keeps a constant value of 12, 14.9 and 17.7 L m^{-2} h^{-1} during the operation for 30 min at the imposed TMP of 0.1, 0.15 and 0.2 bar, respectively. It can be explained that there was little fouling on the membrane surface during this time [40]. When the imposed TMP reached 0.25 bar, the flux decreased exponentially and rapidly from 20 to 16.7 L m^{-2} h^{-1}, suggesting that at this point gradual fouling was occurring. This trend was achieved for the all nanocomposite membranes. However, the permeate flux for nanocomposite membranes was higher than for neat PVC membranes. Among all of nanocomposite membranes, PVC/Al-1.5 shows the highest value in critical flux among other samples. The
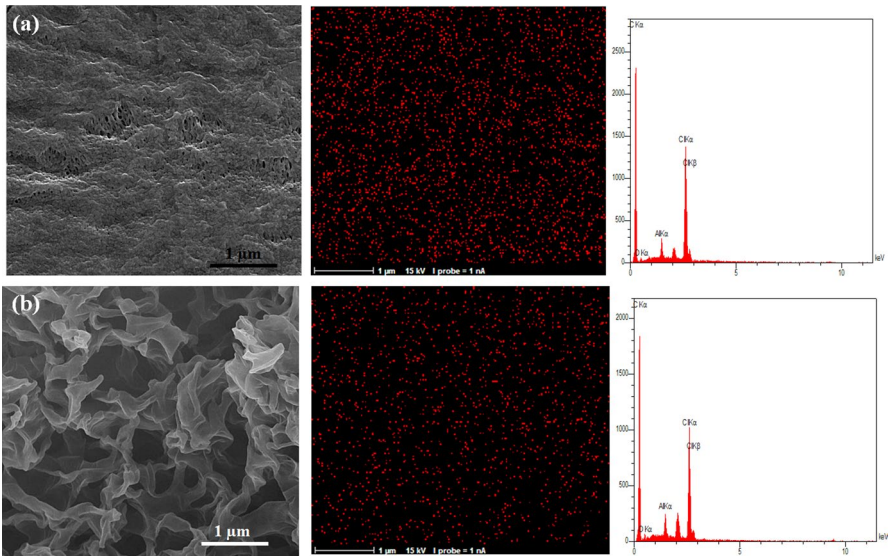
Fig. 5 EDS mapping and EDS graph of **a** surface, **b** cross section of PVC/Al-1.5 nanocomposite membrane
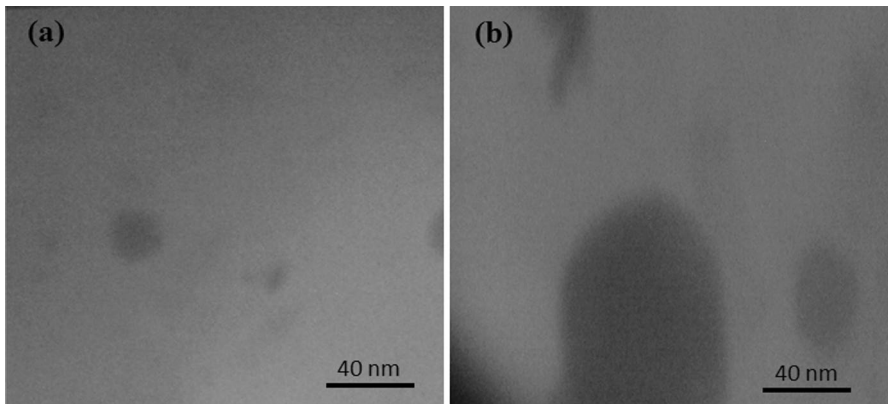
Fig. 6 TEM images of distribution of Al_2O_3 nanoparticles in PVC membrane: **a** 1.5 wt.%, **b** 2 wt.%

hydrophilic Al_2O_3 nanoparticles improved the surface hydrophilicity of the nanocomposite membrane, thereby alleviating interaction between HA foulants and the membrane surface and enhancing the membrane critical flux. On the other hand, the pore size of membranes can affect the permeate flux of membranes under constant TMP. He et al. [41] found that the membranes with the smallest pore size exhibited a serious flux decline for short-term operation. According to the obtained results from the FE-SEM image from the membrane surfaces (Fig. 3), it becomes clear that the surface pore size of the PVC/Al-1.5 nanocomposite membrane is bigger than that of the neat PVC membrane. Therefore, the
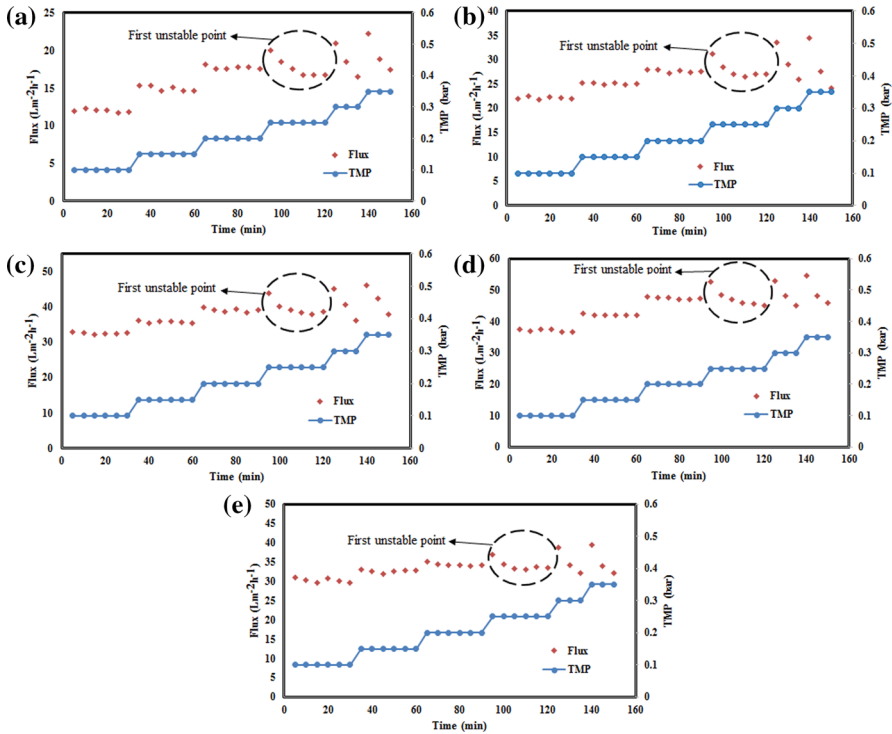
Fig. 7 The critical flux determination of **a** neat PVC, **b** PVC/Al-0.5, **c** PVC/Al-1, **d** PVC/Al-1.5, **e** PVC/Al-2 membranes by the TMP step method

surface pore size plays a significant role in the improvement in the critical flux of PVC/Al-1.5 nanocomposite membrane.

Figure 8 shows variations of TMP and filtration flux during measurement of the critical point. It can be seen that the permeation flux of all membranes increased linearly by increasing TMP. However, after a critical point (critical TMP), the slope of flux variation changed. For all membranes, critical TMP was measured about of 0.2 bar, which corresponds to the critical flux of 17.7, 27.8, 39.1, 47.3 and 34.3 L m^{-2} h^{-1} for neat PVC, PVC/Al-0.5, PVC/Al-1, PVC/Al-1.5 and PVC/Al-2 membranes, respectively. At higher of this point, the compressible of the cake layer formed on the membrane surface and the transport of HA to the membrane surface will increase and the concentration polarization layer or the cake layer will become more compact and thicker, resulting in higher hydraulic resistance against the flow [39].

Membrane performance and antifouling analysis

Figure 9 shows the variation of flux vs. time for neat PVC and nanocomposite membranes under subcritical conditions (TMP = 0.15 bar) for HA filtration. The
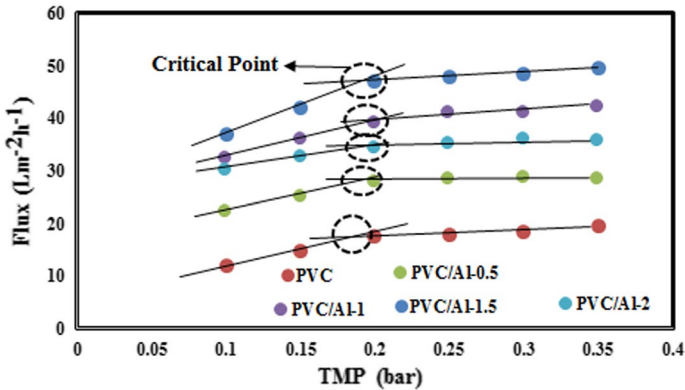
Fig. 8 Variation of filtration flux and TMP for measurement of critical flux
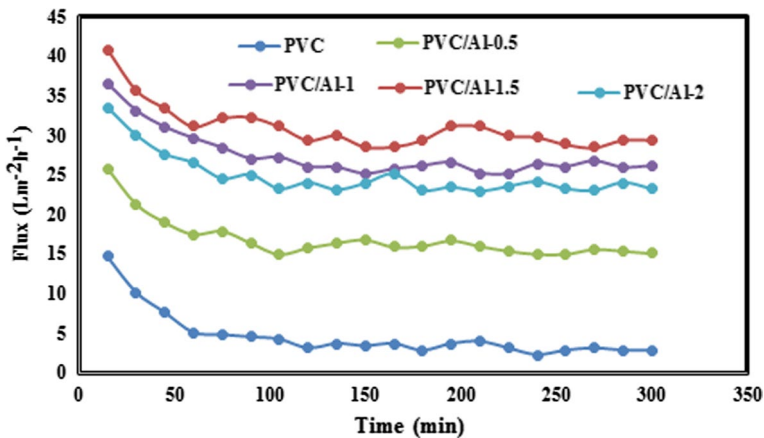

Fig. 9 Permeation flux versus time for neat PVC and nanocomposite membranes under subcritical conditions (TMP = 0.15 bar)

obtained results indicated that the PVC/Al-1.5 nanocomposite membrane exhibited higher flux than the other samples and especially neat PVC membrane. Because of fouling caused by HA molecules, the permeate flux of all membranes rapidly reduced for the first 60 min and then remained constant up to the end of filtration (300 min). HA molecules in the solution can deposit on the membrane surface at the start of the filtration operation. Such adsorbed layer causes a sharp drop in flux during the first few minutes of the operation. As shown in Fig. 9, it can be clearly seen that the initial flux of the PVC/Al-1.5 nanocomposite membrane is higher than that of the neat PVC membrane, which can be attributed to higher porosity, bigger surface pore size and improvement in the hydrophilicity of nanocomposite membrane when compared to the neat PVC membrane. According to Fig. 9, all membranes show a slow decline in the permeate flux, which

corresponds to subcritical conditions operations. If HA filtration was performing under supercritical conditions, the downward trend of the flux would be sharp.

In order to evaluate the fouling mitigation effects quantitatively, the fouling parameters were calculated. Then, the reversible fouling ratio (RFR), the irreversible fouling ratio (IFR), the total fouling ratio (TFR) and the flux recovery ratio (FRR) are summarized in Table 3. It can be seen that the TFR of neat PVC membranes is higher than that of all nanocomposite membranes. Generally, a high value of FRR indicates strong resistance to membrane fouling. As shown in Table 3, the PVC/Al-1.5 nanocomposite membrane has a higher value in FRR than the neat PVC membrane and other nanocomposite membranes. FRR promoted from 39.3% for the neat PVC membrane to 80.7% for the PVC/Al-1.5 membrane, which showed the high antifouling properties of PVC/Al-1.5 nanocomposite membranes.

In addition, IFR values for neat PVC and PVC/Al-1.5 nanocomposite membranes are 60.7% and 19.4%, respectively, which show that the irreversible fouling of PVC membranes significantly improved by adding 1.5 wt.% of Al_2O_3 nanoparticles. According to the literature, a lower IFR demonstrates a better performance in controlling total fouling [42]. Due to the hydrophilic property of hydroxyl groups, hydrophobic materials such as HA are expected not to be attached on OH groups. Thus, Al_2O_3 improved the hydrophilicity of the PVC membrane, which causes fewer hydrophobic materials to be attached on the membrane surfaces.

Hydroxyl groups facilitate hydrogen bonding with water molecules and create a middle water layer between the membrane surface and HA molecules. Creation of this layer restricts the adsorption of HA molecules [42]. Indeed, improvement in the membrane hydrophilicity increases the fouling resistance of the membranes due to the hydrophobic nature of foulants. This phenomenon is shown schematically in Fig. 10.

In addition to the high permeate flux, the modified membranes should be able to reject HA. The obtained results from HA rejection are shown in Table 3. According to Table 3, all nanocomposite membranes show higher HA removal when compared to neat PVC, and in this case, PVC/Al-1.5 nanocomposite membranes reject HA more than 90%, while this value stands at 81.6% for neat PVC membranes. The presence of the OH group on the Al_2O_3 nanoparticle surface decreased the interaction between HA molecules and the membrane surface, and therefore, an improvement in rejection occurred. Addition of Al_2O_3 increases the

Table 3 Fouling parameters and rejection for membranes under subcritical conditions

Membranes	RFR (%)	IFR (%)	TFR (%)	FRR (%)	Rejection (%)
Neat PVC	28.6	60.7	89.3	39.3	81.6
PVC/Al-0.5	26.8	37.2	64	62.8	83.4
PVC/Al-1	25.9	26.8	52.7	73.2	86.9
PVC/Al-1.5	24	19.4	43.4	80.7	90.5
PVC/Al-2	32.7	29.1	61.8	70.9	85.1
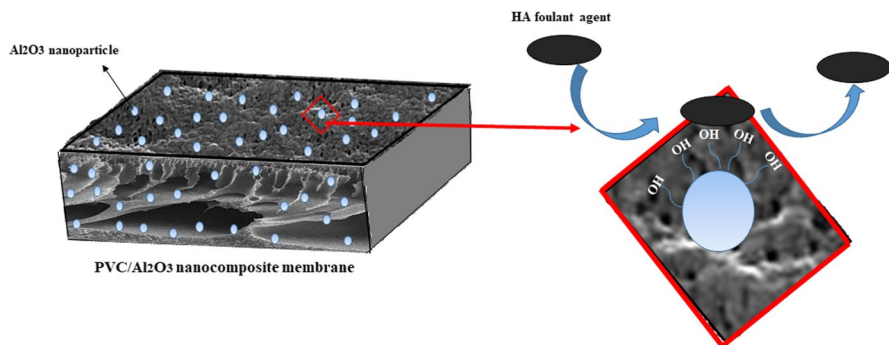
Fig. 10 Schematic representation of reject of HA foulant on the surface of PVC nanocomposite membrane by OH groups on the Al_2O_3 nanoparticles surface

surface hydrophilicity of the membranes, which results in lower affinity and interaction between HA molecules and the membrane surface and higher rejection [27].

Conclusions

PVC/Al_2O_3 nanocomposite membranes were prepared by the phase separation process in order to remove humic acid (HA) from contaminated water in a submerged membrane system. Al_2O_3 nanoparticles at different amounts of 0.5 to 2 wt.% were added to the polymeric casting solution, including PEG 200 Da as a pore former and NMP as a solvent. The FTIR analysis confirmed the presence of the OH group on the surface of nanocomposite membranes. Incorporation of Al_2O_3 nanoparticles, especially 1.5 wt.%, in the PVC membrane, resulted in improvement in hydrophilicity and porosity when compared to the neat PVC membrane. FE-SEM images indicated that remarkable changes in the PVC nanocomposite membrane surface occurred and the nanocomposite membrane showed high surface porosity with a larger surface pore size. Also, FE-SEM images from the nanocomposite membrane showed bigger macrovoids than those from the neat PVC membrane.

The obtained results from critical flux revealed that Al_2O_3 led to an increase in the critical flux of the membranes from 17.7 L m^{-2} h^{-1} for the neat PVC membrane to 47.3 L m^{-2} h^{-1} for the PVC/Al-1.5 nanocomposite membrane, mainly due to an increase in the surface pore size and the higher surface hydrophilicity of the nanocomposite membrane. It was shown that lower TFR, IFR and higher permeate flux for nanocomposite membrane confirm the advantages of the modified membrane, which was attributed to hydrophilicity. HA rejection for PVC/Al-1.5 nanocomposite membrane was higher than 90%, while only 81.6% removal efficiency was obtained for the neat PVC membrane.

References

1. Caprarescu S, Miron AR, Purcar V, Radu AL, Sarbu A, Ianchis R, Erbasu DI (2017) Commercial goose-berry buds extract containing membrane for removal of methylene blue dye from synthetic wastewaters. Rev Chim (Bucharest) 68:1757

2. Caprarescu S, Radu AL, Purcar V, Sarbu A, Vaireanu DI, Ianchis R, Ghiurea M (2014) Removal of copper ions from simulated wastewaters using different bicomponent polymer membranes. Water Air Soil Pollut 225:2079

3. Caprarescu S, Miron AR, Purcar V, Radu AL, Sarbu A, Nicolae CA, Pascu M, Ion-Ebrasu D, Raditoiu V (2018) Treatment of Crystal violet from synthetic solution using membranes doped with natural fruit extract. Clean-Soil Air Water 46:1700413

4. Ion-Ebrasu D, Pollet BG, Spinu-Zaulet A, Soare A, Carcadea E, Varlam M, Caprarescu S (2019) Graphene modified fluorinated cation-exchange membranes for proton exchange membrane water electrolysis. Int J Hydrog Energy 44:10190–10196

5. Chang H, Qu F, Liu B, Yu H, Li K, Shao S, Li G, Liang H (2015) Hydraulic irreversibility of ultrafiltration membrane fouling by humic acid: effects of membrane properties and backwash water composition. J Membr Sci 493:723–733

6. Jhaveri JH, Patel CM, Murthy Z (2017) Preparation, characterization and application of GO–TiO$_2$/PVC mixed matrix membranes for improvement in performance. J Ind Eng Chem 52:138–146

7. Caprarescu S, Miron AR, Purcar V, Radu AL, Sarbu A, Ion-Ebrasu D, Atanase LI, Ghiurea M (2016) Efficient removal of Indigo Carmine dye by a separation process. Water Sci Technol 74: 2462–2473.

8. Costa AR, de Pinho MN (2005) Effect of membrane pore size and solution chemistry on the ultrafiltration of humic substances solutions. J Membr Sci 255:49–56

9. Xia S, Yao L, Zhao Y, Li N, Zheng Y (2015) Preparation of graphene oxide modified polyamide thin film composite membranes with improved hydrophilicity for natural organic matter removal. Chem Eng J 280:720–727

10. Fu X, Maruyama T, Sotani T, Matsuyama H (2008) Effect of surface morphology on membrane fouling by humic acid with the use of cellulose acetate butyrate hollow fiber membranes. J Membr Sci 320:483–491

11. Hao Y, Moriya A, Maruyama T, Ohmukai Y, Matsuyama H (2011) Effect of metal ions on humic acid fouling of hollow fiber ultrafiltration membrane. J Membr Sci 376:247–253

12. Hamid N, Ismail A, Matsuura T, Zularisam A, Lau W, Yuliwati E, Abdullah M (2011) Morphological and separation performance study of polysulfone/titanium dioxide (PSF/TiO$_2$) ultrafiltration membranes for humic acid removal. Desalination 273:85–92

13. Etemadi H, Yegani R, Babaeipour V (2017) Performance evaluation and antifouling analyses of cellulose acetate/nanodiamond nanocomposite membranes in water treatment. J Appl Polym Sci 134:21

14. Ekambaram K, Doraisamy M (2017) Fouling resistant PVDF/Carboxymethyl chitosan composite nanofiltration membranes for humic acid removal. Carbohydr Polym 173:431–440

15. Behboudi A, Jafarzadeh Y, Yegani R (2018) Enhancement of antifouling and antibacterial properties of PVC hollow fiber ultrafiltration membranes using pristine and modified silver nanoparticles. J Environ Chem Eng 6:1764–1773

16. Rabiee H, Vatanpou V, Farahani MHDA, Zarrabi H (2015) Improvement in flux and antifouling properties of PVC ultrafiltration membranes by incorporation of zinc oxide (ZnO) nanoparticles. Sep Purif Technol 156:299–310

17. Wang SY, Fang LF, Cheng L, Jeon S, Kato N, Matsuyama H (2018) Novel ultrafiltration membranes with excellent antifouling properties and chlorine resistance using a poly (vinyl chloride)-based copolymer. J Membr Sci 549:101–110

18. Behboudi A, Jafarzadeh Y, Yegani R (2016) Preparation and characterization of TiO$_2$ embedded PVC ultrafiltration membranes. Chem Eng Res Des 114:96–107

19. Demirel E, Zhang B, Papakyriakou M, Xia S, Chen Y (2017) Fe$_2$O$_3$ nanocomposite PVC membrane with enhanced properties and separation performance. J Membr Sci 529:170–184

20. Zhao Y, Lu J, Liu X, Wang Y, Lin J, Peng N, Li J, Zhao F (2016) Performance enhancement of polyvinyl chloride ultrafiltration membrane modified with graphene oxide. J Colloid Interface Sci 480:1–8

21. Etemadi H, Shojaei A (2014) Characterization of reinforcing effect of alumina nanoparticles on the novolac phenolic resin. Polym Compos 35:1285–1293

22. Homayoonfal M, Mehrnia MR, Rahmani S, Mojtahedi YM (2015) Fabrication of alumina/polysulfone nanocomposite membranes with biofouling mitigation approach in membrane bioreactors. J Ind Eng Chem 22:357–367

23. Saleh TA, Gupta VK (2012) Synthesis and characterization of alumina nano-particles polyamide membrane with enhanced flux rejection performance. Sep Purif Technol 89:245–251

24. Yan L, Hong S, Li ML, Li YS (2009) Application of the Al_2O_3–PVDF nanocomposite tubular ultrafiltration (UF) membrane for oily wastewater treatment and its antifouling research. Sep Purif Technol 66:347–352

25. Ghazanfari D, Bastani D, Mousavi SA (2017) Preparation and characterization of poly (vinyl chloride) (PVC) based membrane for wastewater treatment. J Water Process Eng 16:98–107

26. Huang H, Lee N, Young T, Gary A, Lozier JC, Jacangelo JG (2007) Natural organic matter fouling of low-pressure, hollow-fiber membranes: Effects of NOM source and hydrodynamic conditions. Water Res 41:3823–3832

27. Rabiee H, Farahani MHDA, Vatanpour V (2014) Preparation and characterization of emulsion poly (vinyl chloride)(EPVC)/TiO_2 nanocomposite ultrafiltration membrane. J Membr Sci 472:185–193

28. Zhang M, Field RW, Zhang K (2014) Biogenic silver nanocomposite polyethersulfone UF membranes with antifouling properties. J Membr Sci 471:274–284

29. Gesan-Guiziou G, Wakeman R, Daufin G (2002) Stability of latex crossflow filtration: cake properties and critical conditions of deposition. Chem Eng J 85:27–34

30. Etemadi H, Yegani R, Seyfollahi M (2017) The effect of amino functionalized and polyethylene glycol grafted nanodiamond on anti-biofouling properties of cellulose acetate membrane in membrane bioreactor systems. Sep Purif Technol 177:350–362

31. Zhao S, Wang P, Wang C, Sun X, Zhang L (2012) Thermostable PPESK/TiO_2 nanocomposite ultrafiltration membrane for high temperature condensed water treatment. Desalination 299:35–43

32. Safarpour M, Khataee A, Vatanpour V (2015) Effect of reduced graphene oxide/TiO_2 nanocomposite with different molar ratios on the performance of PVDF ultrafiltration membranes. Sep Purif Technol 140:32–42

33. Zhang F, Zhang W, Yu Y, Deng B, Li J, Jin J (2013) Sol–gel preparation of PAA-g-PVDF/TiO_2 nanocomposite hollow fiber membranes with extremely high water flux and improved antifouling property. J Membr Sci 432:25–32

34. Xu Z, Zhang J, Shan M, Li Y, Li B, Niu J, Zhou B, Qian X (2014) Organosilane-functionalized graphene oxide for enhanced antifouling and mechanical properties of polyvinylidene fluoride ultrafiltration membranes. J Membr Sci 458:1–13

35. Hong J, He Y (2014) Polyvinylidene fluoride ultrafiltration membrane blended with nano-ZnO particle for photo-catalysis self-cleaning. Desalination 332:67–75

36. Wang Z, Yu H, Xia J, Zhang F, Li F, Xia Y, Li Y (2012) Novel GO-blended PVDF ultrafiltration membranes. Desalination 299:50–54

37. Zinadini S, Zinatizadeh AA, Rahimi M, Vatanpour V, Zangeneh H (2014) Preparation of a novel antifouling mixed matrix PES membrane by embedding graphene oxide nanoplates. J Membr Sci 453:292–301

38. Amini M, Etemadi H, Akbarzadeh A, Yegani R (2017) Preparation and performance evaluation of high-density polyethylene/silica nanocomposite membranes in membrane bioreactor system. Biochem Eng J 127:196–205

39. Etemadi H, Yegani R, Seyfollahi M, Babaeipour V (2017) Preparation and performance evaluation of cellulose acetate/nanodiamond nanocomposite membrane in the treatment of pharmaceutical wastewater by membrane bioreactor. Desalin Water Treat 76:98–111

40. Fox R, Stuckey D (2015) The effect of sparging rate on transmembrane pressure and critical flux in an AnMBR. J Environ Manag 151:280–285

41. He Y, Xu P, Li C, Zhang B (2005) High-concentration food wastewater treatment by an anaerobic membrane bioreactor. Water Res 39:4110–4118

42. Vatanpour V, Naeeni RSE, Ghadimi A, Karami A, Sadatnia B (2018) Effect of detonation nanodiamond on the properties and performance of polyethersulfone nanocomposite membrane. Diam Relat Mater 90:244–255

Publisher's Note Springer Nature remains neutral with regard to jurisdictional claims in published maps and institutional affiliations.